Title:

Genome editing of *Capsaspora owczarzaki* suggests an ancestral function of the Hippo signaling effector YAP/TAZ/Yorkie in cytoskeletal dynamics but not proliferation

Authors:

Jonathan E Phillips[1], Maribel Santos[1], Mohammed Kanchwala[2], Chao Xing[2], Duojia Pan[1*]

Affiliations:

[1]Department of Physiology, Howard Hughes Medical Institute, University of Texas Southwestern Medical Center, Dallas, Texas 75390, USA

[2]Eugene McDermott Center for Human Growth & Development, Departments of Bioinformatics and Clinical Sciences, University of Texas Southwestern Medical Center, Dallas, Texas 75390, USA

* correspondence: duojia.pan@utsouthwestern.edu

Abstract:

Many genes that function in animal development are present in the close unicellular relatives of animals, but little is known regarding the premetazoan function of these genes. Here, we develop techniques for genetic manipulation in the filasterean *Capsaspora owczarzaki* and use these tools to characterize the *Capsaspora* ortholog of the Hippo signaling nuclear effector YAP/TAZ/Yorkie (coYki). In contrast to its potent oncogene activity in metazoans, we show that coYki is dispensable for cell proliferation but regulates cytoskeletal dynamics and the morphology of multicellular aggregates in *Capsaspora*. Our results suggest an ancestral role for the Hippo pathway in cytoskeletal regulation, which was later co-opted to regulate cell proliferation in animals.

One Sentence Summary: Gene disruption in a unicellular holozoan suggests an ancestral role for YAP/TAZ/Yorkie in cytoskeletal regulation and cell aggregation but not cell proliferation.

Main text:

The vast morphological diversity observed in animals is generated by developmental programs mediated by a surprisingly small set of conserved signaling pathways (*1*). An exciting and unexpected finding from comparative genomic analysis indicates that many components of these pathways are present in the closest unicellular relatives of animals (*2*). This finding raises the question of whether these genes show similar functions in animals and their unicellular relatives, and, if not, what the ancestral functions of these

genes were, and how they evolved to function in multicellular processes in animals. Answering this question could illuminate the roots of animal multicellularity and provide novel perspective on how to manipulate the activity of these biomedically important pathways.

One such signaling pathway is the Hippo pathway, which coordinates cell proliferation, differentiation, and survival in animals. Initially defined as a tumor suppressor pathway that restricts tissue growth in *Drosophila* development, Hippo signaling plays a conserved role in organ size control and regeneration in mammals *(3, 4)*. This pathway comprises a core kinase cascade involving sequential activation of two kinases, Hpo/MST and Wts/LATS, which culminates in the phosphorylation and inactivation of the potent growth-stimulatory transcriptional coactivator Yorkie/YAP/TAZ (*5*). This core kinase cascade is in turn regulated by diverse upstream inputs, most notably mechanical force, the state of the actin cytoskeleton, and cell-cell or cell-substrate adhesion as part of a mechanotransduction pathway that relays mechanical and architectural cues to gene expression (*6*). Echoing its pervasive function in metazoan growth control, the Hippo pathway is required for contact-inhibition of proliferation in cultured mammalian cells (*7*), and defective Hippo signaling leading to YAP/TAZ oncogene activation is a major driver of human cancers (*8*).

The Hippo pathway was at one point thought to be specific to animals. However, recent genome sequencing efforts have revealed that a core Hippo pathway and many known upstream regulators are encoded in the genomes of the closest unicellular relatives of

63 animals such as choanoflagellates and filasterians (*9*). The choanoflagellates are
64 flagellated filter feeders that can form multicellular rosette structures by incomplete
65 cytokinesis (*10*), whereas filasterians are amoeboid organisms characterized by actin-
66 rich filopodial projections (Fig. 1, A and B) and represent the most basal known unicellular
67 organism encoding all core components of the Hippo pathway (*9*). *Capsaspora*
68 *owczarzaki* is a filasterean originally isolated as a putative endosymbiont in the freshwater
69 snail *B. glabrata* that can attack and kill the parasitic schistosome *S. mansoni* (*11*).
70 *Capsaspora* can be cultured easily in growth medium containing protein source and
71 serum in adherent or shaking culture and can be transiently transfected, allowing for the
72 examination of protein localization using fluorescent fusion proteins (*12*). Although
73 *Capsaspora* tends to grow as a unicellular organism in laboratory culture conditions,
74 under certain conditions *Capsaspora* cells can adhere to each other to form multicellular
75 aggregates (Fig. 1, C to E, (*13*)), suggesting that multicellular behaviors may have been
76 selected for in the lineage leading to *Capsaspora*. Previously, we have shown that
77 overexpression of *Capsaspora* Hippo pathway components such as CoYki and CoHpo in
78 *Drosophila* elicits similar phenotypes as their *Drosophila* counterpart (*9*), suggesting that
79 a biochemically active Hippo signaling pathway likely evolved well before the emergence
80 of Metazoa. Besides the Hippo pathway, the *Capsaspora* genome encodes homologues
81 of other key regulators of animal development such as components of the integrin
82 adhesome (*14*), cadherins (*15*), tyrosine kinases such as Src and Abl (*16*), NF-kB (*17*)
83 and p53 (*18*). Thus, *Capsaspora* offers a unique opportunity to elucidate the ancestral
84 function of these important developmental regulators in a close unicellular relative of
85 animals.

In an effort to make *Capsaspora* a tractable system for evolutionary cell biology studies, we developed genetic tools for overexpression and loss-of-function analysis. We first established a method for engineering stable *Capsaspora* cell lines by transfecting a vector encoding the fluorescent protein mScarlet and resistance to the antibiotic Geneticin (GenR). After transfection, antibiotic selection, and generation of clonal lines by serial dilution, we were able to generate uniformly mScarlet-positive clonal populations of cells (Fig. 1F**)**. Besides GenR, transfection of *Capsaspora* with genes encoding resistance to nourseothricin (NatR) or hygromycin (HygR) followed by selection with the respective antibiotic could also generate drug-resistant transformants (fig. S1). These results demonstrate that stable *Capsaspora* cell lines expressing multiple transgenes can be generated.

We next sought to develop tools for loss-of-function analysis in *Capsaspora*. After unsuccessful attempts with CRISPR-Cas9-mediated genome editing, possibly due to the lack of nonhomologous end joining machinery components in *Capsaspora*, we used homologous recombination for gene disruption by replacing each allele of a diploid *Capsaspora* gene with a distinct selectable antibiotic marker (Fig. 1G). This strategy allowed us to generate a cell line in which both *coYki* alleles were disrupted (fig. S2), with no detectable expression of the deleted region of *coYki* **(**Fig. 1, H to J**)**. These results demonstrate the generation of a homozygous *coYki* disruption mutant (subsequently *coYki -/-*) and establish a method for the generation of mutants by gene targeting in *Capsaspora.*

To determine the effect of loss-of-coYki on cell proliferation, we examined the proliferation of *Capsaspora* cells in adherent or shaking culture. In contrast to what may be expected based on previous studies in animal cells, we observed no significant difference in cell proliferation between WT and *coYki -/-* cells in either condition (Fig. S3). We next sought to examine cell proliferation within *Capsaspora* aggregates. Previously, aggregates have been generated by gentle shaking of cell cultures (*13*). To make aggregates more amenable to extended imaging *in situ*, we developed a condition that induced robust aggregate formation by plating *Capsaspora* cells in low-adherence wells (Fig. 1, C to E). Under this condition, most cells coalesced into aggregates over 2-3 days, leaving few isolated cells in the culture. Treatment with the calcium chelator EGTA resulted in rapid dissociation of the aggregates (fig. S4), suggesting that calcium-dependent cell adhesion mediates aggregate integrity. We used EdU incorporation to label proliferating cells in aggregates, and observed no significant difference in the percent of EdU-positive cells between WT and *coYki -/-* genotypes (Fig. 2, A and B). Unlike clones of cultured mammalian cells that often display increased cell proliferation at the clonal boundary (*19*), distribution of EdU+ cells was homogeneous within *Capsaspora* aggregates (Fig. 2A), suggesting that a mechanism akin to contact-mediated inhibition of proliferation is absent in *Capsaspora*. Together, these results suggest that the rate of proliferation of *Capsaspora* is independent of YAP/TAZ/Yorkie or contact inhibition.

While examining *Capsaspora* aggregates, we observed a profound phenotype in the shape of the *coYki -/-* aggregates. After aggregate induction by plating cells in low-

adherence conditions, WT cell aggregates showed a round morphology (Fig. 2C). In contrast, *coYki -/-* aggregates were asymmetric and less circular than WT aggregates (Fig. 2D). Computational analysis of aggregate morphology and size revealed that WT and *coYki -/-* aggregate size was not significantly different (Fig. 2E), whereas *coYki -/-* aggregates were significantly less circular than WT aggregates (Fig. 2F). Optical sectioning of aggregates expressing mScarlet showed that WT aggregates were thicker perpendicular to the culture surface and more spherical than *coYki -/-* aggregates (Fig. 2G). Time-lapse microscopy of aggregation over a period of six days showed that, whereas WT cells accreted into round aggregates that fused with other aggregates when in close proximity but never underwent fission, *coYki -/-* aggregates were dynamically asymmetrical, showed a progressive reduction in circularity, and occasionally underwent fission (movie S1). Taken together, these findings uncover a critical role for coYki in social interactions underlying aggregate morphology, but not cell proliferation, in *Capsaspora*.

Cell-cell adhesion and cell-substrate adhesion affect the morphology and stability of tumor cell aggregates (*20, 21*). We therefore tested whether cell-cell adhesion and cell-substrate adhesion differ in WT *and coYki -/- cells.* A prediction of differential cell-cell adhesion is that mosaic aggregates of WT and *coYki -/-* cells may show cell sorting within aggregates (*22*). To test this prediction, we induced aggregate formation after mixing mCherry-labeled WT or *coYki* -/- cells with unlabeled WT cells at 1:9 ratio. The distribution of mCherry-labeled WT or *coYki* -/- cells within such mixed aggregates was similar and no cell sorting was evident (fig. S5)**,** indicating that individual *coYki -/-* cells are competent to adhere to and integrate within aggregates and suggesting that the aberrant morphology

of *coYki -/-* aggregates is an emergent property of a large number of *coYki -/-* cells. To further test whether cell-cell adhesion differs in WT and *coYki -/-* cells, we vigorously vortexed *Capsaspora* culture to separate individual cells, allowed cell clumps to form by cell-cell adhesion under gentle rotation, and then counted the number of cells in each clump. Numbers of cells per clump were similar for WT and *coYki -/-* cells (fig. S6A), suggesting that the occurrence of cell-cell adhesion is similar in these genotypes. We next tested whether cell-substrate adhesion differed in WT and *coYki -/-* cells by agitating cultures of adherent cells and counting the number of cells that disassociate from the culture surface. After agitation, significantly more *coYki* -/- cells remained attached to the culture surface compared to WT cells (fig. S6B), indicating that coYki negatively regulates cell-substrate adhesion. Together, our data suggest that coYki affects the morphology of cell aggregates by affecting cell-substrate adhesion but not cell-cell adhesion.

To characterize properties of *coYki -/-* cells that may contribute to abnormal aggregate morphology, we used time-lapse microscopy to examine the dynamic morphology of individual WT and *coYki -/-* cells in adherent culture. Interestingly, the cortices of *coYki -/-* cells were much more dynamic than those of WT cells. Whereas *coYki -/-* cells display extensive membrane protrusions and retractions, such dynamic membrane structures were rarely observed in WT cells (movie S2). To characterize the differences in cell membrane dynamics, we quantified the occurrence of cell protrusions in WT cells, *coYki -/-* cells, and *coYki -/-* cells expressing a *coYki* rescue transgene. WT cells rarely showed protrusions. In contrast, *coYki -/-* cells showed an average of 3.1 protrusions per minute (Fig. 3A), a phenotype that was rescued in *coYki -/-* cells expressing a *coYki* transgene

(Fig. 3A, movie S3). These results suggest that coYki affects the cortical dynamics of *Capsaspora* cells.

In principle, the extensive membrane protrusions made by *coYki -/-* cells may represent F-actin-rich pseudopodia, which drive amoeboid motility, or, alternatively, F-actin-poor blebs, which are actin-depleted extensions of plasma membrane generated by disassociation of the membrane from the cell cortex or cortical rupture (*23*). To distinguish between these possibilities, we stably expressed a fusion protein of the F-actin-binding Lifeact peptide (*24*) with mScarlet in WT and *coYki -/-* cells and examined F-actin dynamics by time-lapse microscopy in adherent cells. At the basal side of WT cells, Lifeact-mScarlet was often enriched at the cell edge corresponding to the direction of cell movement, suggesting that *Capsaspora* undergoes F-actin-mediated amoeboid locomotion (movie S4). As cells move, some Lifeact-mScarlet signal appears as stationary foci on the basal surface, suggesting the existence of actin-rich structures that mediate cell-substrate interaction in *Capsaspora* (Fig. 3B, movie S4). Optical sections at mid-height of WT cells showed that F-actin was enriched at a circular cell cortex, where transient bursts of small F-actin puncta were often observed (Fig. 3B, movie S5). In contrast, cortical shape was less circular in *coYki -/-* cells, and F-actin concentration along the cortex was less uniform (Fig. 3B). During the formation of the membrane protrusions produced by *coYki -/-* cells, F-actin was initially depleted as compared to the rest of the cell (Fig. 3C, movie S6). After the membrane protrusions had fully extended, F-actin accumulated first at the distal end and then along the entire cortex of the protrusion, followed by the regression of the protrusion. A similar sequence of cytoskeletal events

occurs in blebbing mammalian cells (*25*). These results suggest that the protrusions observed in *coYki -/-* cells are actin-depleted blebs, and that after bleb formation, F-actin re-accumulates within the bleb leading to cortical reformation and bleb regression.

To determine whether the abnormal cortical cytoskeleton is specific to *coYki -/-* cells in adherent culture, we examined *coYki -/-* cells within aggregates by time-lapse microscopy. Lifeact-mScarlet-expressing cells were mixed with cells stably expressing the green fluorescent protein Venus so that Lifeact-mScarlet-expressing cells were well-spaced and able to be imaged individually. As in adherent cells, *coYki -/-* cells within aggregates showed dynamic formation of actin-depleted blebs (movie S7). Thus, *coYki -/-* cells show aberrant cortical cytoskeleton and excessive membrane blebbing in both isolated adherent cells and within aggregates.

Loss of coYki causes both bleb-like protrusions and abnormal aggregate morphology, suggesting that the cellular phenotypes observed in *coYki -/-* cells (membrane blebbing and related cortical cytoskeletal defects) may underlie the aberrant aggregate morphology. We tested this hypothesis by treating *coYki -/-* cells with Blebbistatin, a myosin II inhibitor named after its bleb-inhibiting activity in mammalian cells (*26*). Strikingly, not only did low concentrations of Blebbistatin suppress the formation of blebs in *coYki -/-* cells (Fig. 3D, movie S8), Blebbistatin also rescued the abnormal morphology of *coYki -/-* aggregates (Fig. 3E). Whereas *coYki -/-* cell aggregates were asymmetric and showed low circularity (Fig. 3E’’’), *coYki -/-* aggregates treated with blebbistatin were circular and resembled WT aggregates (Fig. 3E’’’’ and 3F). These results suggest a

causal link between the membrane/cytoskeletal defects observed in individual *coYki -/-* cells and the abnormal morphology of *coYki -/-* aggregates.

To characterize the transcriptional targets of coYki that may underlie the morphological/cytoskeletal defects of *coYki -/-* cells, we performed RNAseq on WT and *coYki -/-* cells in adherent culture. This analysis revealed 1205 differentially expressed genes, including 397 downregulated and 808 upregulated genes in the *coYki* mutant. Functional enrichment analysis of these two gene sets revealed distinct enrichment of functional categories (Fig. 4, A and B). Genes predicted to encode actin-binding proteins were enriched in the set of genes upregulated in the *coYki -/-* mutant, suggesting that these genes may play a role in the aberrant cytoskeletal dynamics observed in *coYki -/- cells.* To further inquire into the potential function of coYki-regulated genes, we searched the 1205 differentially expressed genes against a previously reported *Capsaspora* phylome (*27*) to identify 638 *Capsaspora* genes with predicted human or mouse orthologs. Ingenuity Pathway Analysis of this mammalian ortholog set showed that the two most significantly enriched functional categories corresponded to cell movement and cell migration (Fig. 4C). Notably, regulation of cell migration was reported as the most enriched functional category among YAP target genes in glioblastoma cells (*28*), and cell motility was an enriched category in an integrative analysis of gene regulatory networks downstream of YAP/TAZ utilizing transcriptomic and cistromic data from multiple human tissues (*29*). However, in contrast to functional enrichment studies in metazoan systems examining genes regulated by Yorkie/YAP/TAZ (*28, 30, 31*), no enrichment was detected

246 in functional categories of cell proliferation or the cell cycle (Fig. 4C). This finding is
247 consistent with the lack of a proliferative phenotype in *coYki -/-* cells.

248

249 In summary, we show that coYki regulates cytoskeletal dynamics and potentially other
250 cortical actin-related processes but is dispensable for the proliferation of *Capsaspora*
251 cells. Such coYki-dependent cortical cytoskeletal function, in turn, regulates the
252 morphology of *Capsaspora* aggregates in a manner that may involve tuning the strength
253 of cell-substrate adhesion. Although the natural history of *Capsaspora*, including the
254 selective advantage of cell aggregation, is poorly understood, our findings suggest that
255 cytoskeletal regulation represents an ancestral function of the Hippo pathway predating
256 the origin of Metazoa, and this pathway was later co-opted to control cell proliferation
257 after the unicellular-to-multicellular transition. Given that the cortical cytoskeleton is both
258 an important upstream regulator and a downstream effector of Hippo signaling in animal
259 cells (*32, 33*), the co-option of the Hippo pathway for cell proliferation control in early
260 metazoans may have provided a convenient mechanism that couples cell proliferation
261 with cytoskeletal and mechanical properties of the cells. Besides illuminating an ancestral
262 function of the Hippo pathway, the genetic tools we have developed for modifying the
263 *Capsaspora* genome provide an unprecedented opportunity to interrogate the
264 premetazoan functions of other developmental regulators that are present in the genomes
265 of close unicellular relatives of animals.

266

267 **References and Notes:**

268 1. A. Pires-daSilva, R. J. Sommer, The evolution of signalling pathways in animal
269 development. *Nat Rev Genet* **4**, 39-49 (2003).

2. N. Ros-Rocher, A. Perez-Posada, M. M. Leger, I. Ruiz-Trillo, The origin of animals: an ancestral reconstruction of the unicellular-to-multicellular transition. *Open Biol* **11**, 200359 (2021).

3. S. Wu, J. Huang, J. Dong, D. Pan, hippo encodes a Ste-20 family protein kinase that restricts cell proliferation and promotes apoptosis in conjunction with salvador and warts. *Cell* **114**, 445-456 (2003).

4. K. F. Harvey, C. M. Pfleger, I. K. Hariharan, The Drosophila Mst ortholog, hippo, restricts growth and cell proliferation and promotes apoptosis. *Cell* **114**, 457-467 (2003).

5. J. Huang, S. Wu, J. Barrera, K. Matthews, D. Pan, The Hippo signaling pathway coordinately regulates cell proliferation and apoptosis by inactivating Yorkie, the Drosophila Homolog of YAP. *Cell* **122**, 421-434 (2005).

6. Y. Zheng, D. Pan, The Hippo Signaling Pathway in Development and Disease. *Dev Cell* **50**, 264-282 (2019).

7. B. Zhao *et al.*, Inactivation of YAP oncoprotein by the Hippo pathway is involved in cell contact inhibition and tissue growth control. *Genes Dev* **21**, 2747-2761 (2007).

8. Y. Wang *et al.*, Comprehensive Molecular Characterization of the Hippo Signaling Pathway in Cancer. *Cell Rep* **25**, 1304-1317 e1305 (2018).

9. A. Sebe-Pedros, Y. Zheng, I. Ruiz-Trillo, D. Pan, Premetazoan origin of the hippo signaling pathway. *Cell Rep* **1**, 13-20 (2012).

10. S. R. Fairclough, M. J. Dayel, N. King, Multicellular development in a choanoflagellate. *Curr Biol* **20**, R875-876 (2010).

11. H. H. Stibbs, A. Owczarzak, C. J. Bayne, P. DeWan, Schistosome sporocyst-killing Amoebae isolated from Biomphalaria glabrata. *J Invertebr Pathol* **33**, 159-170 (1979).

12. H. Parra-Acero *et al.*, Transfection of Capsaspora owczarzaki, a close unicellular relative of animals. *Development* **145**, (2018).

13. A. Sebe-Pedros *et al.*, Regulated aggregative multicellularity in a close unicellular relative of metazoa. *Elife* **2**, e01287 (2013).

14. A. Sebe-Pedros, A. J. Roger, F. B. Lang, N. King, I. Ruiz-Trillo, Ancient origin of the integrin-mediated adhesion and signaling machinery. *Proc Natl Acad Sci U S A* **107**, 10142-10147 (2010).

15. S. A. Nichols, B. W. Roberts, D. J. Richter, S. R. Fairclough, N. King, Origin of metazoan cadherin diversity and the antiquity of the classical cadherin/beta-catenin complex. *Proc Natl Acad Sci U S A* **109**, 13046-13051 (2012).

16. H. Suga *et al.*, Genomic survey of premetazoans shows deep conservation of cytoplasmic tyrosine kinases and multiple radiations of receptor tyrosine kinases. *Sci Signal* **5**, ra35 (2012).

17. L. M. Williams, T. D. Gilmore, Looking Down on NF-kappaB. *Mol Cell Biol* **40**, (2020).

18. A. Sebe-Pedros, B. M. Degnan, I. Ruiz-Trillo, The origin of Metazoa: a unicellular perspective. *Nat Rev Genet* **18**, 498-512 (2017).

19. H. W. Fisher, J. Yeh, Contact inhibition in colony formation. *Science* **155**, 581-582 (1967).

20. A. F. Blandin *et al.*, Glioma cell dispersion is driven by alpha5 integrin-mediated cell-matrix and cell-cell interactions. *Cancer Lett* **376**, 328-338 (2016).

21. L. Saias, A. Gomes, M. Cazales, B. Ducommun, V. Lobjois, Cell-Cell Adhesion and Cytoskeleton Tension Oppose Each Other in Regulating Tumor Cell Aggregation. *Cancer Res* **75**, 2426-2433 (2015).

22. R. A. Foty, M. S. Steinberg, The differential adhesion hypothesis: a direct evaluation. *Dev Biol* **278**, 255-263 (2005).

23. G. Charras, E. Paluch, Blebs lead the way: how to migrate without lamellipodia. *Nat Rev Mol Cell Biol* **9**, 730-736 (2008).

24. J. Riedl *et al.*, Lifeact: a versatile marker to visualize F-actin. *Nat Methods* **5**, 605-607 (2008).

25. G. T. Charras, C. K. Hu, M. Coughlin, T. J. Mitchison, Reassembly of contractile actin cortex in cell blebs. *J Cell Biol* **175**, 477-490 (2006).

26. A. F. Straight *et al.*, Dissecting temporal and spatial control of cytokinesis with a myosin II Inhibitor. *Science* **299**, 1743-1747 (2003).

27. A. Sebe-Pedros *et al.*, High-Throughput Proteomics Reveals the Unicellular Roots of Animal Phosphosignaling and Cell Differentiation. *Dev Cell* **39**, 186-197 (2016).

28. C. Stein *et al.*, YAP1 Exerts Its Transcriptional Control via TEAD-Mediated Activation of Enhancers. *PLoS Genet* **11**, e1005465 (2015).

29. M. Paczkowska *et al.*, Integrative pathway enrichment analysis of multivariate omics data. *Nat Commun* **11**, 735 (2020).

30. A. Ikmi *et al.*, Molecular evolution of the Yap/Yorkie proto-oncogene and elucidation of its core transcriptional program. *Mol Biol Evol* **31**, 1375-1390 (2014).

31. F. Zanconato *et al.*, Genome-wide association between YAP/TAZ/TEAD and AP-1 at enhancers drives oncogenic growth. *Nat Cell Biol* **17**, 1218-1227 (2015).

32. H. Deng *et al.*, Spectrin couples cell shape, cortical tension, and Hippo signaling in retinal epithelial morphogenesis. *J Cell Biol* **219**, (2020).

33. B. G. Fernandez *et al.*, Actin-Capping Protein and the Hippo pathway regulate F-actin and tissue growth in Drosophila. *Development* **138**, 2337-2346 (2011).

34. H. Parra-Acero *et al.*, Integrin-Mediated Adhesion in the Unicellular Holozoan Capsaspora owczarzaki. *Curr Biol* **30**, 4270-4275 e4274 (2020).

35. D. S. Bindels *et al.*, mScarlet: a bright monomeric red fluorescent protein for cellular imaging. *Nat Methods* **14**, 53-56 (2017).

36. D. M. Veltman, G. Akar, L. Bosgraaf, P. J. Van Haastert, A new set of small, extrachromosomal expression vectors for Dictyostelium discoideum. *Plasmid* **61**, 110-118 (2009).

37. S. S. Lehman *et al.*, Versatile nourseothricin and streptomycin/spectinomycin resistance gene cassettes and their use in chromosome integration vectors. *J Microbiol Methods* **129**, 8-13 (2016).

38. S. H. Park *et al.*, Generation and application of new rat monoclonal antibodies against synthetic FLAG and OLLAS tags for improved immunodetection. *J Immunol Methods* **331**, 27-38 (2008).

39. S. J. Charette, P. Cosson, Preparation of genomic DNA from Dictyostelium discoideum for PCR analysis. *Biotechniques* **36**, 574-575 (2004).

40. S. Andrews, FastQC: a quality control tool for high throughput sequence data. . *Available online at: http://www.bioinformatics.babraham.ac.uk/projects/fastqc*, (2010).

41. S. Wingett, FastQ Screen: quality control tool to screen a library of sequences in FastQ format against a set of sequence databases. . *Available online at: http://www.bioinformatics.babraham.ac.uk/projects/fastq_screen*, (2011).

42. A. Dobin *et al.*, STAR: ultrafast universal RNA-seq aligner. *Bioinformatics* **29**, 15-21 (2013).

43. Y. Liao, G. K. Smyth, W. Shi, featureCounts: an efficient general purpose program for assigning sequence reads to genomic features. *Bioinformatics* **30**, 923-930 (2014).

44. M. D. Robinson, D. J. McCarthy, G. K. Smyth, edgeR: a Bioconductor package for differential expression analysis of digital gene expression data. *Bioinformatics* **26**, 139-140 (2010).

45. J. Huerta-Cepas, S. Capella-Gutierrez, L. P. Pryszcz, M. Marcet-Houben, T. Gabaldon, PhylomeDB v4: zooming into the plurality of evolutionary histories of a genome. *Nucleic Acids Res* **42**, D897-902 (2014).

46. E. Paradis, K. Schliep, ape 5.0: an environment for modern phylogenetics and evolutionary analyses in R. *Bioinformatics* **35**, 526-528 (2019).

47. A. Kramer, J. Green, J. Pollard, Jr., S. Tugendreich, Causal analysis approaches in Ingenuity Pathway Analysis. *Bioinformatics* **30**, 523-530 (2014).

48. W. Huang da, B. T. Sherman, R. A. Lempicki, Bioinformatics enrichment tools: paths toward the comprehensive functional analysis of large gene lists. *Nucleic Acids Res* **37**, 1-13 (2009).

Acknowledgements:

We thank the McDermott Sequencing Core and the Next-Generation Sequencing Core for RNA sequencing, and Dr. Iñaki Ruiz-Trillo for sharing information on *Capsaspora* vectors.

Funding: This work was supported in part by National Institute of Health grant EY015708 to D.P. During this work J.E.P was a Howard Hughes Medical Institute fellow of the Life Sciences Research Foundation. D.P. is an investigator of the Howard Hughes Medical Institute.

Author Contributions: JEP and DP conceived the study and designed experiments. JEP and MS performed experiments. JEP, MK, and CX analyzed RNAseq data. JEP, DP, and MK wrote the original manuscript draft. JEP, MS, DP, MK, and CX revised and edited the manuscript.

Competing interests: Authors declare that they have no competing interests.

403 **Data and materials availability:** RNAseq data generated in this study have been
404 deposited into the NCBI SRA (Bioproject PRJNA759885). The following plasmids have
405 been deposited at Addgene: pJP72 (#176479), pJP102 (#176480), pJP103 (#176481),
406 and pJP118 (#176494).
407
408

409 **Supplementary Materials**

410 Materials and methods

411 Figs. S1 to S6

412 References 34 to 48

413 Movies S1 to S8

414 Data S1 to S3

415

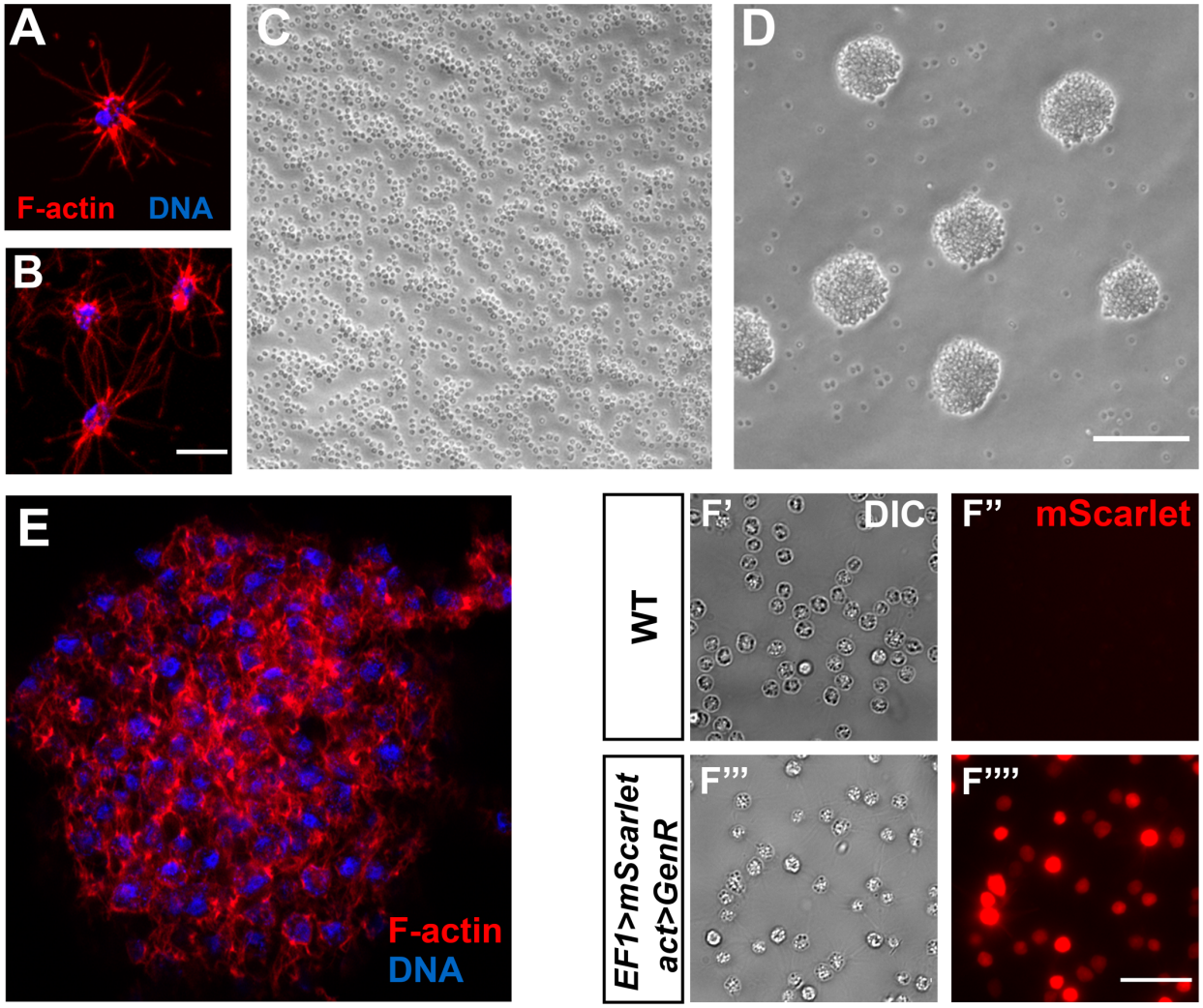

Fig. 1. Stable transgene expression and gene knockout in *Capsaspora*. (A) A solitary *Capaspora* cell showing thin F-actin-enriched projections. Phalloidin and DAPI are used to stain F-actin and DNA, respectively. **(B)** Cells at higher densities can contact other cells through projections. Scale bar is 5 microns. **(C-D)** *Capsapsora* cells were diluted to 7.5 x 10^5 cells/mL and inoculated into either a standard polystyrene culture plate **(C)** or a low-adherence plate **(D).** At 3 days, cells in standard plates grow as a monolayer whereas cells in low-adherence plates form round aggregates. **(E)** An aggregate stained for F-actin shows actin-rich connections between cells within an aggregate. Scale bar is 10 microns. (**F)** WT *Capsaspora* cells and a clonal population of cells stably expressing mScarlet were imaged to show fluorescence. Scale bar is 20 microns. **(G)** Strategy for disrupting the *coYki* gene by homologous recombination. GenR, geneticin resistance cassette; TBD, Tead-binding domain; WW, WW domain. **(H)** Strategy for demonstrating disruption of *coYki* by qPCR. Amplicon 1 corresponds to a region of the *coYki* gene that should be absent in a homozygous mutant, whereas Amplicon 2 corresponds to a segment of the gene 3' of the region targeted for deletion. **(I-J)** qPCR of Amplicons 1 and 2 in WT and putative *coYki -/-* cells. The differences between WT and *coYki -/-* for both Amplicons 1 and 2 are significant (t-test).

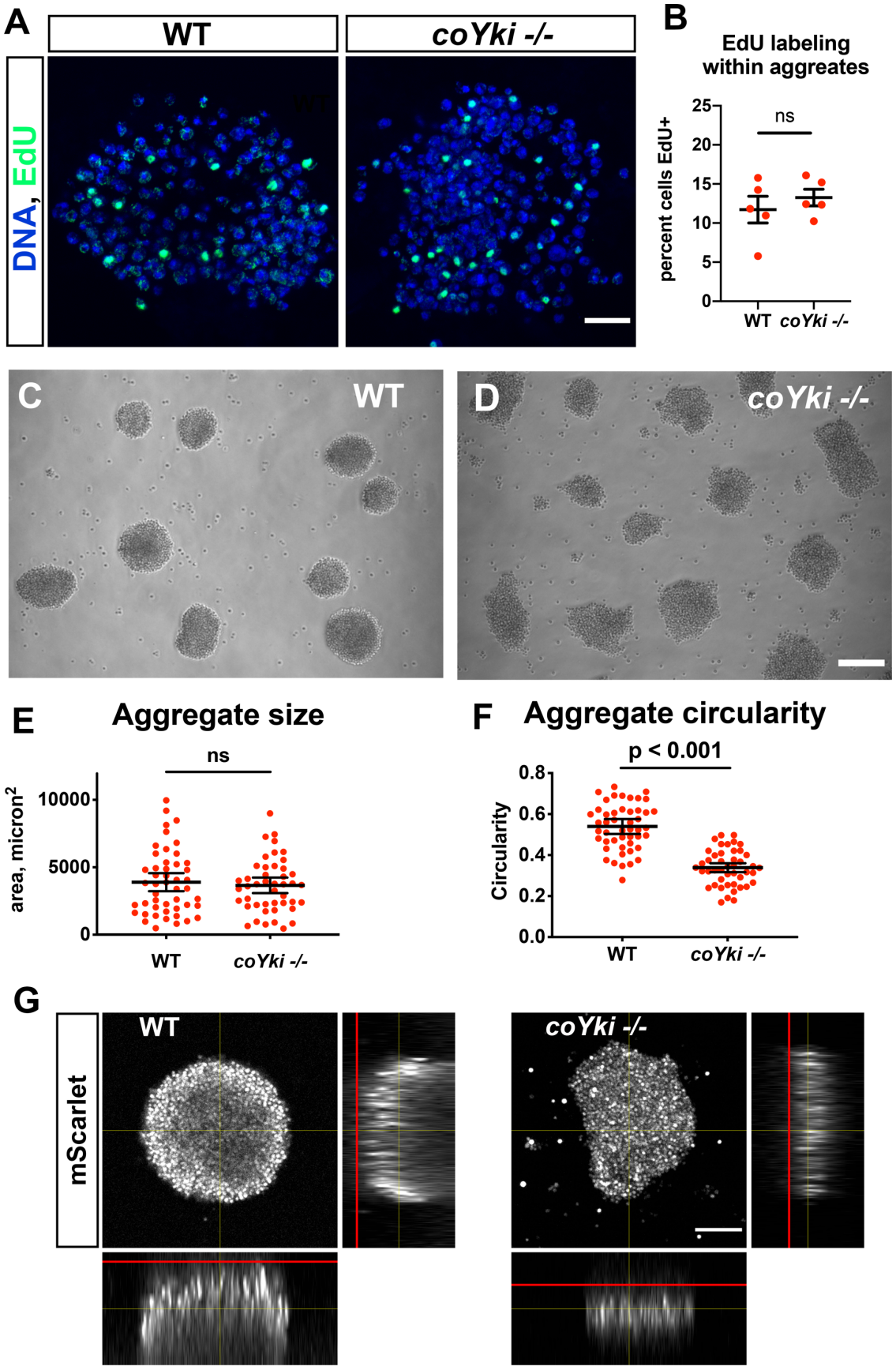

438

Fig. 2. Loss of coYki results in no apparent effect on cell proliferation but alters the morphology of multicellular aggregates. (A) To examine proliferation within aggregates, EdU was used to label proliferating cells within aggregates grown in low-adherence plates. **(B)** The percent of cells positive for EdU within aggregates was quantified. Each red circle indicates measurement results for a single aggregate, and mean ± SEM is shown in black. The difference between WT ant *coYki -/-* cells is not significant (t-test). **(C-D)** WT or *coYki -/-* cells were innoculated into low-adherence plates, and cell aggregates were imaged at 5 days. Scale bar is 75 microns. **(E-F)** Aggregate size and circularity was measured from aggregate images using ImageJ. The difference in aggregate circularity between WT and *coYki -/-* is significant (t-test). Bars indicate the mean ± SEM (n=3 with 15 aggregates measured for each independent experiment), and dots indicate values for individual aggregates. **(G)** Orthogonal views of WT and *coYki -/-* aggregates are shown. Cell aggregates stably expressing mScarlet were imaged live by confocal microscopy. Red lines show the location of the culture surface. Scale bar is 50 microns.

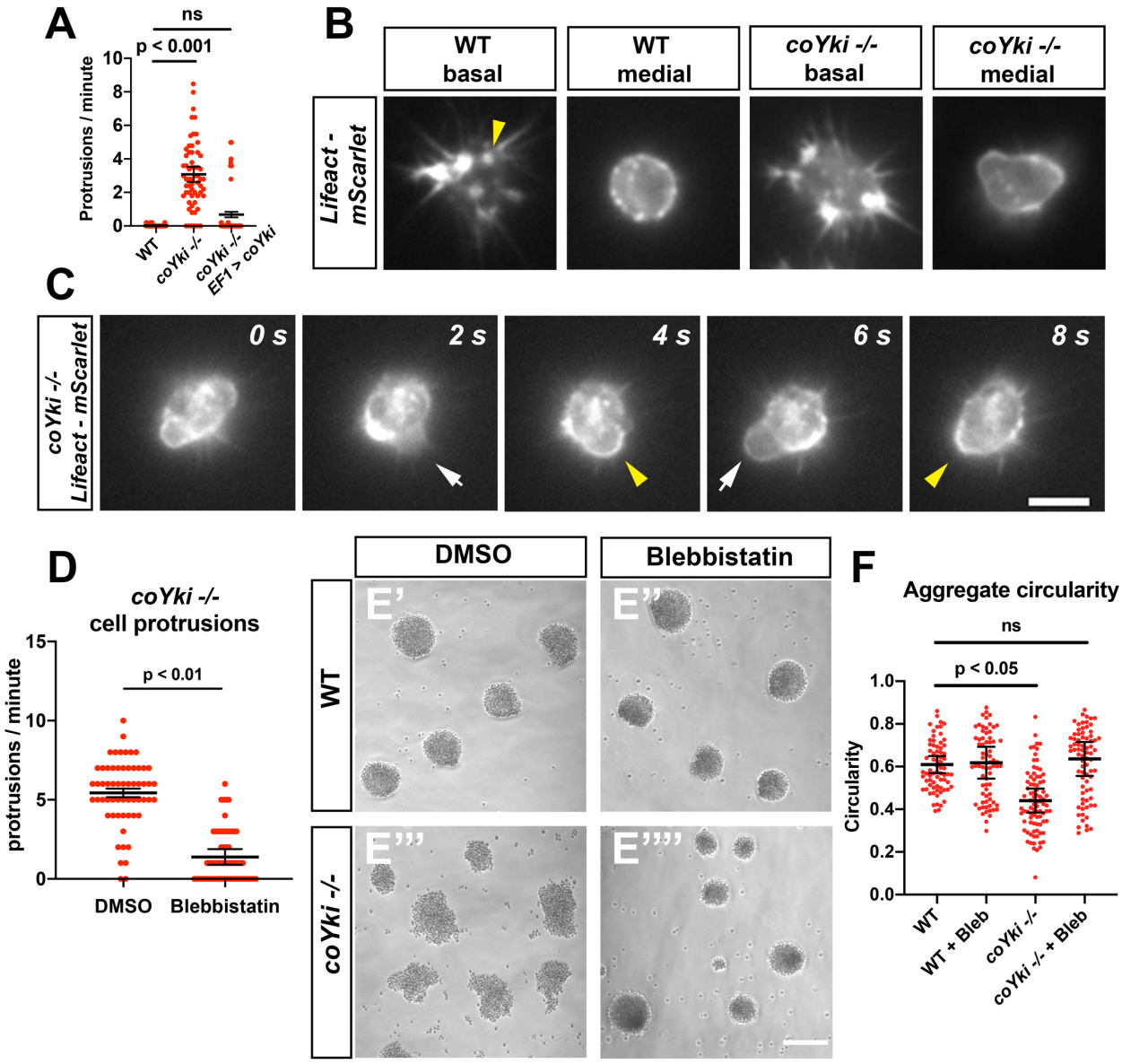

Fig. 3. Loss of coYki results in bleb-like distortions at the cell cortex. (A) *Capsaspora* cells on a glass surface were imaged by time-lapse microscopy and individual cells were scored for number of protrusions per minute. A protrusion is defined as a localized extension of the cell boundary that disrupts a previously inert region of the cortex and/or changes the direction of movement of the cell. Differences between WT and *coYki -/-* are significant (one-way ANOVA, Tukey's test). Values from 3 independent experiments with

20 cells measured for each condition per experiment are shown. Red dots indicate the measurement from an individual cell, and black bars indicate the mean ± SEM of the means from each independent experiment. **(B)** Cells on a glass surface stably expressing Lifeact-mScarlet were imaged focusing on the base of the cell at the substrate ("basal") or at the mid-height of the cell ("medial"). Arrowhead shows an example of Lifeact signal at the base of the cell that remains stationary as the cell moves (see Movie S4). Scale bar is 5 microns. **(C)** Time series of a *coYki -/-* cell stably expressing Lifeact-mScarlet on a glass surface. White arrows indicate Lifeact-depleted bleb-like protrusions, and yellow arrowheads indicate areas of cell cortex constriction, which correlate with increased Lifeact signal. Scale bar is 5 microns. **(D)** Cells on a glass surface were treated with DMSO or 1 μM blebbistatin for 1 hour, and then cells were imaged by time lapse microscopy and the number of protrusions per cell was quantified. **(E)** Cells were inoculated into low-adherence plates with DMSO **(E',E''')** or 1 μM blebbistatin **(E'',E'''')**, and aggregates were imaged after 5 days. Scale bar is 75 microns. **(F)** Circularity of aggregates was measured with ImageJ using images of aggregates from the indicated conditions. Black bars indicate the mean ± SEM (n=4 with 15 aggregates measured for each independent experiment), and red dots indicate the measurements for individual aggregates. Differences in circularity between WT and *coYki -/-* aggregates treated with DMSO are significant (one-way ANOVA, Dunnett's test), whereas differences between WT aggregates treated with DMSO and *coYki -/-* aggregates treated with blebbistatin are not. "Bleb" indicates blebbistatin.

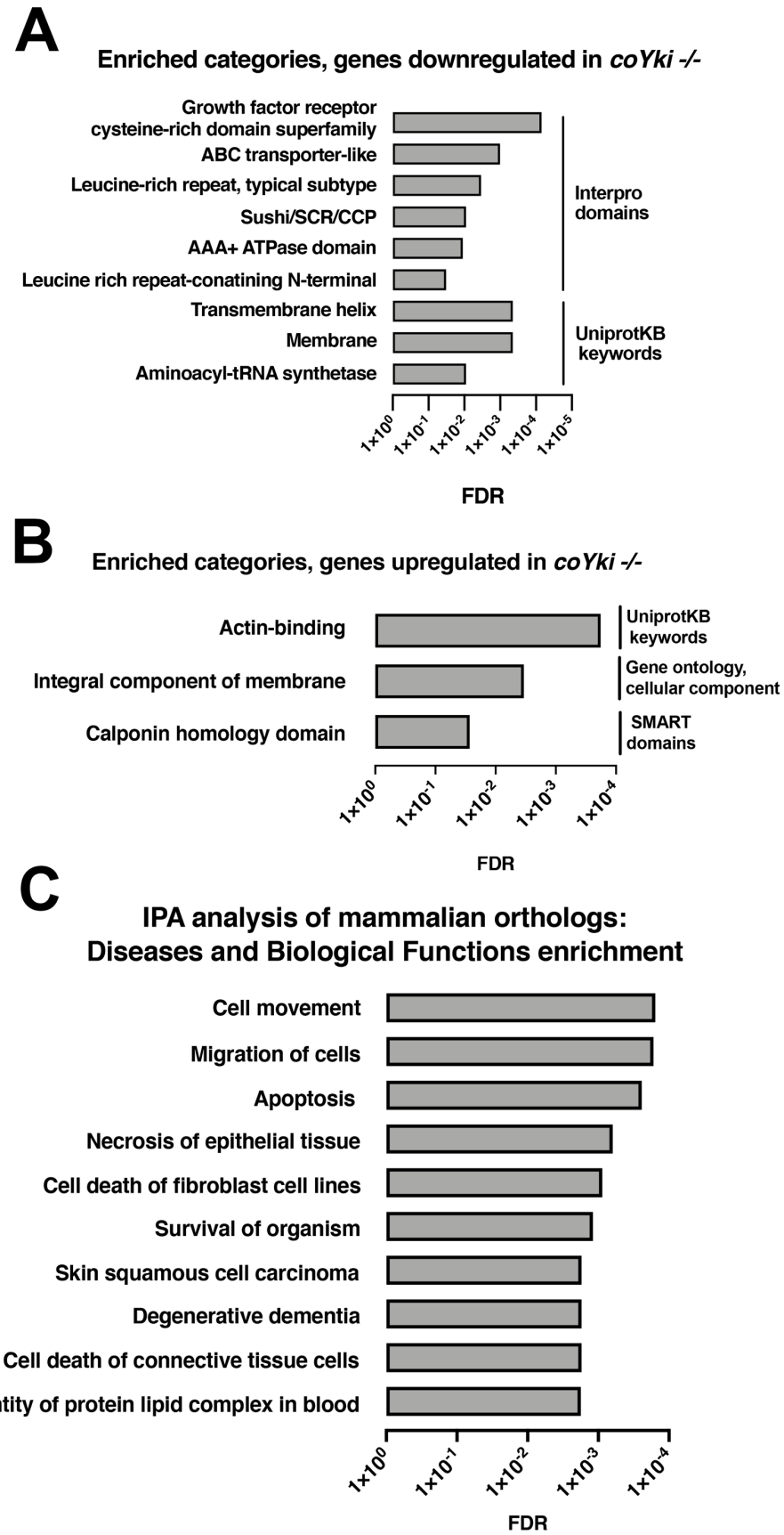

488

Fig. 4. Functional enrichment of genes differentially expressed in *coYki -/-* cells. Top enriched categories from the sets of genes significantly downregulated **(A)** or upregulated **(B)** in *coYki -/-* cells compared to WT are shown. **(C)** Ingeneuity Pathway Analysis was performed on a set of predicted human/mouse orthologs of *Capsaspora* genes with significant changes in expression in *coYki -/-* cells. Enriched diseases and biological functions with false discovery rate (FDR) ≤ 0.05 are shown.

Supplementary Materials for

Genome editing of *Capsaspora owczarzaki* suggests an ancestral function of the Hippo signaling effector YAP/TAZ/Yorkie in cytoskeletal dynamics but not proliferation

Jonathan E Phillips, Mohammed Kanchwala, Chao Xing, and Duojia Pan

Correspondence to: duojia.pan@utsouthwestern.edu

This PDF file includes:

Materials and Methods
Figs. S1 to S6
Captions for Movies S1 to S8
Captions for Data S1 to S3

Other Supplementary Materials for this manuscript include the following:

Movies S1 to S8
Data S1 to S3:

Data S1. Sequences of synthesized gene fragments used in this study
Data S2. Sequences of oligonucleotides used in this study
Data S3. Plasmids constructed for this study

Materials and Methods

Cell culture

Capsaspora cells were maintained in ATCC Medium 1034 (modified PYNFH medium) supplemented with 25 µg/mL Ampicillin (referred to below as "growth medium") in a 23°C incubator. Cells were kept in either 25 cm^2 cell culture flasks in 8 mL medium or in 75 cm^2 cell culture flasks in 15 ml medium. To induce cell aggregation, cells were resuspended to 7.5 x 10^5 cells/ml in growth medium, and 1 ml of this cell suspension was added per well to a 24-well ultra-low attachment plate (Sigma CLS3473). To test the effect of blebbistatin on aggregate morphology, a 20 mM stock solution of blebbistatin (Sigma B0560) in DMSO was made, and cells were resuspended to 7.5 x 10^5 cells/ml in growth medium with 1 µm blebbistatin or DMSO only as a vehicle control. Aggregates were then generated as described above and imaged with a Nikon Eclipse Ti inverted microscope with NIS-Elements acquisition software.

To characterize cell proliferation during growth on a solid substrate, *Capsaspora* cells were diluted to 1 x 10^5 cells/ml in growth medium, and 800 µl of this dilution was pipetted into multiple wells in a 24-well polystyrene cell culture plate. To prevent edge effects, wells at the edge of the plate were not used and were instead filled with 800 µl of water. The plates were then kept in in a 23°C incubator. Each day, 1.5 µl of a 500 mM EDTA solution was added to a well, and cells in the well were resuspended by pipetting up and down for one minute. Resuspended cells were then transferred to a 1.5 mL tube, vortexed, and then the cell density was determined by hemocytometer. To characterize cell proliferation in shaking culture, cells were diluted to 1 x 10^5 cells/ml in growth medium,

and 20 ml of this dilution was added to a 125 ml Erlenmeyer culture flask. Cultures were then incubated in an orbital shaker at 150 rpm and 23°C. Cell density was determined daily by transferring 200 µl of culture to a 1.5 ml tube, adding 1.5 µl of 500 mM EDTA solution to disassociate any aggregated cells, vortexing, and counting by hemocytometer.

Fixation and staining of aggregates

To fix and stain aggregates, aggregates were generated as described above, and then aggregates were collected from a 24-well plate by gentle pipetting. 500 µl of aggregate suspension was added dropwise to 9 ml of PM PFA (100 mM PIPES ph 6.9, 0.1 mM $MgSO_4$, 4% PFA filtered through a 0.45 µm syringe filter) in a 15 mL polystyrene tube, and tubes were left undisturbed for 1 hour to allow fixation. Aggregates were then centrifuged at 1000 x g for 3 minutes and resuspended in 500 µl of PEM buffer (100 mM PIPES pH 6.9, 1 mM EGTA, 0.1 mM $MgSO_4$). After transferring aggregates to a microcentrifuge tube, aggregates were centrifuged for 2000 x g for 2 minutes, the supernatant was removed, and aggregates were resuspended in 300 µl of PEM.

As we found that aggregates were fragile during continued centrifugation-resuspension cycles, we developed a protocol where solution changes could be done without centrifugation using 24-well plate inserts with an 8 micron pore membrane at the insert base (Corning 3422). Before use with aggregates, 100 µl PEM buffer was added to a well in a 24-well plate, 300 µl of PEM was added to a membrane insert, and the insert was placed in the well and allowed to drain (contact between the membrane and the solution within the well is critical for draining). Aggregates in 300 µl of PEM were added to the

insert, and the insert was moved to a new well with 100 µl of PEM and allowed to drain. As a wash step, the membrane insert was then moved to a well containing 1200 µl of PEM, allowing the membrane insert to fill with PEM buffer, and after a 5 minute incubation, the membrane was moved to a new well with 100 µl of PEM and allowed to drain. The membrane insert was then moved to a well containing 1200 µl of PEM block/permeabilization solution (100 mM PIPES pH 6.9, 1 mM EGTA, 0.1 mM $MgSO_4$, 1% BSA, 0.3% Triton X-100) and incubated for 30 minutes at room temperature. The membrane insert was moved to a well with 100 µl of PEM and allowed to drain and then moved into a well containing 1 mL PEM with DAPI (2 µg/mL) and Phalloidin (0.1 µM) and incubated for 15 minutes at room temperature. Aggregates were then washed once more in 1200 µl PEM. To mount aggregates for imaging, the membrane insert was placed in a new well with 100 µl of PEM buffer and was allowed to drain, aggregates were resuspended in the residual buffer (approximately 50 µl) by gentle pipetting, and then aggregates were pipetted onto a microscope slide and allowed to settle for 5 minutes. Kimwipes were then placed in contact with the edge of the liquid on the slide, allowing for removal of excess buffer by capillary action. 15 µl of Fluoromount G (SouthernBiotech) was pipetted onto the aggregates, which were then covered with a 22 x 40 mm cover glass and sealed with nail polish. Aggregates were subsequently imaged with a Zeiss LSM 880 confocal microscope. Staining of adherent cells with phalloidin was done as previously described (*34*).

<u>EdU labeling of aggregates</u>

To examine cell proliferation within aggregates by EdU labeling, aggregates were generated in ultra-low adherence 24-well plates as described above. 3 days after aggregation was initiated, 100 µl of growth medium containing EdU was added to aggregates to result in a 150 µM EdU concentration. Aggregates were incubated with EdU for 4 hours and then fixed and resuspended in 300 µl PEM buffer as described above. Aggregates were then processed for imaging following the manufacturer's protocol (ThermoFisher C10339) using the 24-well plate membrane insert method described above to transfer aggregates between solutions. For all steps, wells with 1 mL of solution were used for washing or staining cells in membrane inserts, and wells with 100 µl of solution were used to drain wells in preparation for transfer into the next solution.

Molecular Biology

For the sequences of synthesized DNA fragments and oligonucleotides used in this study, see Data S1 and S2, respectively. For a list of plasmids generated for this study, see Data S3. To generate a vector for mScarlet expression in *Capsaspora* (pJP71), a DNA construct containing an open reading frame encoding the mScarlet protein (*35*) codon-optimized for expression in *Capsaspora* and under control of the previously described EF1-α promoter and terminator from the pONSY-mCherry vector (*12*) was constructed by gene synthesis (sJP1) and cloned into the EcoRV site of the pUC57-mini vector (Genscript). A KpnI site and an AflII site were incorporated at the beginning and end of the coding sequence, respectively, allowing for the construction of N or C-terminal protein fusion constructs by Gibson assembly. To generate a plasmid for expression of mScarlet and a Geneticin resistance gene (pJP72), the NeoR coding sequence from the

620 *Dictyostelium* pDM323 vector (*36*) was codon optimized for *Capsaspora*, the optimized
621 sequence was synthesized with the promoter and terminator from the *Capsaspora* actin
622 ortholog gene CAOG_06018, and the synthesized fragment (sJP2) was cloned into the
623 SmaI site of pJP71 by Gibson assembly. To generate plasmids expressing mScarlet and
624 either nourseothricin resistance (pJP102) or hygromycin resistance (pJP103), an identical
625 strategy to that used in constructing pJP72 was used, except either a synthesized codon-
626 optimized nourseothricin acetyltransferase gene (sJP3) based on the sequence of
627 pUC18T-mini-Tn7T-nat (*37*) or a synthesized codon-optimized hygromycin B
628 phosphotransferase gene (sJP4) based on the sequence of *Dictyostelium* vector pDM358
629 (*36*) was used.
630
631 To generate a plasmid encoding coYki and Hygromycin resistance for rescue of *coYki -/-*
632 phenotypes (pJP119), a DNA fragment encoding coYki and a c-terminal OLLAS epitope
633 tag (*38*) was generated by PCR from a synthesized a gene encoding the coYki protein
634 (sJP5) using primers oJP101 and oJP102. To limit recombination of the transgene with
635 the endogenous coYki loci, we recoded the coYki reading frame using synonymous codon
636 replacement, resulting in a coYki gene with 73 percent nucleotide similarity to the WT
637 coYki gene but encoding an identical polypeptide. This PCR product was then cloned into
638 a KpnI and AflII digest of pJP103 using Gibson assembly.
639
640 To generate a plasmid encoding a Lifeact-mScarlet fusion protein and hygromycin
641 resistance (pJP118), a DNA fragment optimized for expression in *Capsaspora* encoding
642 the Lifeact peptide (*24*) (sJP6) was synthesized and cloned into the KpnI site of pJP103

by Gibson assembly. To generate a plasmid expressing Venus and Geneticin resistance (pJP114), the Venus reading frame was amplified from $p_{EF1\alpha}$ -CoH2B:Venus (Addgene #111877, (*12*)) using primers oJP103 and oJP104 and cloned into a KpnI and AflII digest of pJP72 by Gibson assembly.

Capsaspora Transfection

24-well plates were prepared for transfection by inserting one sterile 12mm circular glass coverslip in each well to aid in cell adhesion during transfection. *Capsaspora* cells at exponential growth phase were collected by pipetting medium over attached cells, resuspended to 7.5 x 10^5 cells/ml in growth medium, and then 800 µl of this cell culture was added per well to the prepared 24-well plate. Cells were incubated at 23°C overnight. The following day growth medium was removed from cells and was replaced by 800 µl of transfection medium (Scheider's Drosophila Medium (ThermoFisher 21720024) with 10% FBS (Thermofisher 26140079) supplemented with 25 µg/mL Ampicillin). After a 10-minute incubation at room temperature, transfection medium was removed from the cells and replaced with 500 of fresh transfection medium. Transfection mixes were then prepared: 100 µl of Opti-MEM I Reduced Serum Medium (ThermoFisher) was added to a 1.5ml tube, and 1 µg of transfecting DNA was added to this medium (for multiple plasmids, an equivalent amount of each plasmid by mass was used). 3 µl of *Trans*IT-X2® transfection reagent (Mirus Bio) was then added to the tube, and the solution was immediately mixed by pipetting up and down. Transfection mixes were incubated at room temperature for 5 minutes, and then 70 µl of the transfection mix was added dropwise to one well in the 24-well plate. Cells were incubated at 23°C for 24 hours, and then the medium was removed

and replaced with 800 µl of growth medium. To image fluorescent transient transfectants, cells were then resuspended by pipetting up and down, and 300 µl of resuspended cells in growth medium were transferred to a well of an 8-well chambered coverglass slide (Nunc). Cells were then imaged 48 hours after addition of growth medium using a Zeiss LSM 880 confocal microscope.

Stable expression of transgenes in clonal *Capsaspora* cell lines

Transforming plasmids were linearized by digestion with either ScaI-HF® or AseI restriction enzymes (NEB), which cut within the ampicillin resistance gene, and then purified from solution and resuspended in nuclease-free water. *Capsaspora* cells were transfected with the linearized plasmids using the *Trans*IT-X2® transfection reagent as described above. Two days after growth medium was added to cells following transfection, the growth medium was removed and replaced with 800 µl of growth medium supplemented with selective drugs. Due to observations of variability in cell viability between transfections, three drug concentrations were tested in parallel for each transfection: for Geneticin (ThermoFisher), cells were treated at 40, 60, or 80 µg/ml; for Nourseothricin (GoldBio), cells were treated at 50, 75, or 100 µg/ml; for Hygromycin B (Sigma), cells were treated at 150, 200, or 250 µg/ml. Cells were grown in selective medium for 2 weeks, and medium was changed every 3 days. Following selection, clonal cell populations were generated by resuspending cells in growth medium by pipetting, diluting cells to 3 cells/mL in growth medium, and adding 100 µl of this dilution to 200 µl of growth medium per in a well in a 48-well plate (this procedure generated approximately 10 wells with cell growth for each 48-well plate). To image fluorescence in stably

689 transfected lines, clonal cell populations were transferred into wells in a 4-well glass
690 bottom chamber slide (Nunc), incubated at 23°C for 24 hours, and cells were then imaged
691 using a Nikon Eclipse Ti inverted microscope with NIS-Elements acquisition software.
692
693 Disruption of the Capsaspora *coYki* gene by gene targeting
694 To disrupt *coYki,* we attempted to delete a 228 bp segment of the coYki open reading
695 frame that encodes the predicted Tead-binding domain (*9*) using a PCR-generated gene
696 targeting construct. We designed a pair of primers that amplify the drug resistance
697 markers described above, including the actin (CAOG_06018) promoter and terminator,
698 with 90 bp of homology adjacent to the sequence targeted for deletion at the 5' end of the
699 primers (oJP105 and oJP106). These primers were used to amplify the Geneticin
700 resistance cassette from pJP72 by PCR, the resulting PCR product was gel purified and
701 resuspended in nuclease-free water, and WT *Capsaspora* cells were transfected with this
702 DNA as described above. Clonal populations of drug-resistant transformants were
703 generated as described above, each clone was grown to confluency in one well in a 24-
704 well plate, cells were collected by pipetting up and down, and genomic DNA was prepared
705 following the protocol described below. To genotype potential mutants, we performed
706 diagnostic PCRs on genomic DNA: to test for presence of the WT allele, we used a
707 forward primer with homology to the genome 5' of the *coYki* sequence targeted for
708 deletion (oJP107) and a reverse primer with homology within the sequence targeted for
709 deletion (oJP108). To detect successful deletion, we used oJP107 as a forward primer
710 and a reverse primer with homology to the geneticin resistance gene (oJP109). 40
711 percent of analyzed clones (6 of 15 tested clones) showed a PCR product indicative of

disruption of the *coYki* allele (fig. S2B). However, all clones showed a band indicative of an intact WT *coYki* gene. We therefore reasoned that, at least for the culture conditions used during transfection, *Capsaspora* cells may be diploid.

After the isolation of clonal lines that were heterozygous for *coYki* disruption with the Geneticin resistance marker as indicated by diagnostic PCR, we attempted to disrupt the remaining *coYki* allele using nourseothricin resistance as a marker. pJP102 was used as a template for PCR using primers oJP105 and oJP106 to generate a nourseothricin resistance cassette flanked by homology arms targeting *coYki* for disruption. This construct was used to transfect a Geneticin-resistant heterozygous coYki disruption mutant, and drug selection of transfectants was done as described above using simultaneous selection with 60 µg/ml Geneticin and 75 µg/ml nourseothricin. After generating clonal populations of drug-resistant transformants, diagnostic PCR was done to detect the intact *coYki* allele as described above or a deletion allele containing the nourseothricin resistance gene using primers oJP107 and oJP110. Two cell lines that showed absence of the WT *coYki* allele and presence of both disruption alleles encoding either Geneticin or nourseothricin resistance were used for subsequent phenotypic studies.

To quantify *coYki* gene expression in a putative homozygous *coYki* disruption mutant (*coYki-/-*) by qPCR, 5 x 10^6 WT or *coYki-/-* cells were collected from culture flasks while in growth medium by pipetting up and down, and RNA was isolated using a RNeasy Mini Plus kit (Qiagen). cDNA was made using the iScript cDNA Synthesis Kit (BioRad), qPCR

735 reactions were made using iQ™ SRBR® Green Supermix (BioRad), and qPCR was
736 performed using a CFX96 Touch Real-time PCR detection system (BioRad) with the
737 following primers: oJP111 and oJP112 to detect GAPDH, oJP113 and oJP114 to detect
738 a region of coYki within the sequence targeted for deletion, and oJP115 and oJP116 to
739 detect a region coYki 3' of the sequence targeted for deletion.
740
741 Preparing *Capsaspora* genomic DNA
742 Capsaspora genomic DNA was prepared for PCR analysis following a procedure
743 previously developed for *Dictyostelium discoideum* (*39*). Cells grown in a 24-well or 48-
744 well plate in growth medium were collected by pipetting up and down, pipetted into a 1.5
745 mL tube, centrifuged at 4000 x g for 5 minutes, and resuspended in 20 µl of nuclease-
746 free water. 20 µl of Lysis buffer (50 mM KCl, 10 mM TRIS pH 8.3, 2.5 mM $MgCl_2$, 0.45%
747 NP40, 0.45% Tween 20, and 800 µg/ml Proteinase K added fresh from a 20 mg/ml stock)
748 was added to cells, which were then incubated at room temperature for 5 minutes. Tubes
749 were then placed at 95°C for 5 minutes. After cooling to room temperature, 1 µl of this
750 sample was then used as a template in a 20-µl diagnostic PCR.
751
752 Quantification of aggregate size and circularity
753 ImageJ was used to quantify aggregate size and circularity using aggregate images.
754 Images were converted to 8-bit format, processed twice using the "Smooth" function, and
755 a Threshold was adjusted for each individual image. The Analyze Particles command was
756 then run with a gate for particle size at 400-infinity micron^2 and the "exclude on edges"
757 option selected. The returned values for aggregate area and circularity were then used

for further analysis. Values corresponding to more than one adjacent aggregate interpreted by the algorithm as a single particle were discarded.

Assaying cell-cell adhesion and cell-substrate adhesion

To examine cell-cell adhesion, cells were collected from a culture flask by pipetting growth media over the culture surface, diluted to 1 x 10^6 cells/mL in growth medium, and vortexed to disrupt cell clumps. 1 mL volumes of cell culture were then transferred to 1.5 mL tubes and incubated on a Labquake™ rotator (Thermo) for one hour at room temperature. Cultures were then examined by hemocytometer, and the number of cells in each clump of cells was counted for at least 35 cell clumps for each independent experiment.

To examine cell-substrate adhesion, cells were diluted to 5 x 10^5 cells/mL in growth medium, and 3 mL volumes of culture were transferred per well to 6-well tissue culture-treated polystyrene plates (Sigma CLS3506) and incubated at 23°C for 48 hours. For agitation, plates were then placed on an orbital shaker and shaken at 140 RPM for 10 minutes, and then the medium from each well ("disassociated fraction") was transferred to a separate tube and 3 mL of new growth medium was added to each well. 3 µL of 500 mM EDTA was then added to each well to detach cells from the culture surface, medium was pipetted up and down over the culture surface 20 times, and this resuspension ("adherent fraction") was transferred to a separate tube. Cell densities of the collected fractions were determined by hemocytometer counts, total cell amounts were calculated by adding the cell numbers for disassociated and adherent fractions for each condition, and the percent of adherent cells for each condition was then calculated. As a control to

examine cell-substrate adhesion in the absence of agitation, the above protocol was followed, except the orbital shaker agitation step was omitted.

Time-lapse Microscopy

To image cells by time-lapse transmitted light or fluorescence microscopy, cells were resuspended to 1 x 10^8 cells/ml in growth medium, and 10 µl of this cell suspension was added as a spot in the center of a well in a 4-well chambered coverglass slide (Nunc). After a 1 hour incubation at room temperature to allow the cells to settle, the 10 µl volume of medium was removed, and 1 ml of growth medium was added to the well, resulting in a spot of cells in the center of the well. Cells were incubated at room temperature for 24 hours, a field of view with well-spaced cells was located, and then cells were imaged by time-lapse microscopy using a Nikon Eclipse Ti inverted microscope with NIS-Elements acquisition software. To image the effect of blebbistatin on individual cells, similar imaging of cells was done, except that cells were treated with either DMSO or 1 µm bebbistatin (Sigma B0560) for one hour before imaging. To image aggregates by time-lapse microscopy, aggregates were generated in ultra-low attachment plates as described above. During aggregate formation, 4-well chambered coverglass slides (Nunc) were coated with UltraPure agarose (ThermoFisher) by making a 1% agarose in nuclease-free water mixture, microwaving to dissolve the agarose, adding 800 µl of molten agarose per well, and removing the molten agarose after 10 seconds by aspiration. Coated wells were then allowed to dry at room temperature in a cell culture hood, resulting in a thin coating of agarose. This coating functions to prevent aggregate adhesion to the glass surface. After aggregate formation, aggregates were resuspended in the well by gentle pipetting,

and then an 800 µl volume of resuspended aggregates was transferred into one agarose-coated well in a 4-well chambered coverglass slide. Aggregates were then imaged using a Zeiss LSM 880 confocal microscope.

RNA-seq

To perform RNA-seq on *Capsaspora* cells, WT or *coYki -/-* cells were collected from growth flasks by removing growth medium, adding fresh growth medium, and resuspending cells attached to the flask by pipetting the medium over the surface. Cells were then diluted to 2 x 10^5 cells/mL, and for each genotype two 75 cm^2 culture flasks were prepared by adding 16 mL of culture dilution to each flask. Culture flasks were incubated at 23°C for 2 days, and then cells were collected by pipetting growth medium over attached cells. Cells were collected by centrifugation at 2100 x g for 5 minutes, and then all cells for each genotype were combined, resuspended in 500 µl of growth medium, and transferred to a microcentrifuge tube. RNA was then prepared with the RNEasy Plus Mini Kit (Qiagen) using the QIAshredder spin column (Qiagen) to homogenize the lysate. RNA samples were run on an Agilent Tapestation 4200 to determine level of degradation, thus ensuring only high quality RNA was used (RIN Score 8 or higher). A Qubit® 4.0 Fluorimeter (ThermoFisher) was used to determine the concentration prior to staring library prep. One microgram of total DNAse-treated RNA was then prepared with the TruSeq Stranded mRNA Library Prep Kit (Illumina). Poly-A RNA was purified and fragmented before strand specific cDNA synthesis. cDNA was then A-tailed and indexed adapters were ligated. After adapter ligation, samples were PCR-amplified and purified with AmpureXP beads, then validated again on the Agilent Tapestation 4200. Before

being normalized and pooled, samples were quantified by Qubit then run on an Illumina NextSeq 500 using V2.5 reagents. Three biological replicates were sequenced for each genotype, with 22-31 million reads generated per sample. The fastq files were checked for quality using fastqc (v0.11.2)(*40*) and fastq_screen (v0.4.4)(*41*). Fastq files were mapped to GCF_000151315.2 reference assembly using STAR (*42*). Read counts were then generated using featureCounts (*43*). Trimmed Mean of M-values normalization and differential expression analysis were performed using edgeR (*44*) (false discovery rate (FDR) <=0.05, absolute log2(fold change) >= 0.5, log(counts per million) >=0). Phylogenetic trees were downloaded from PhyloDB (*45*) corresponding to *Capsaspora* (PhyID 101) and pairwise distances for each gene were extracted using an R package ape (*46*). Closest Human and mouse orthologues were then extracted and used to annotate the *Capsaspora* genes. These annotated gene names were then used with IPA (*47*) (QIAGEN Inc., https://www.qiagenbioinformatics.com/products/ingenuity-pathway-analysis) to get significantly enriched pathways in "Diseases and Bio Functions" category. To identify functional enrichment in the sets of genes upregulated or downregulated in *coYki -/-* cells, DAVID Functional Annotation Tool (*48*) was used to identify functional categories with FDR < 0.05 using all *Capsaspora* genome genes as the gene population background.

Statistics

All statistics were done using Prism (GraphPad software, San Diego, CA). Student's t-test was done to compare differences between two groups, and one-way analysis of

849 variance (ANOVA) with a post-hoc test was used to compare differences among groups
850 greater than two.
851
852 Gene nomenclature
853 In the manuscript we use italicized text to refer to a gene (e.g., *coYki)*, unitalicized text
854 to refer to a protein (e.g., coYki), "-/-" to indicate a homozygous deletion mutant (e.g.,
855 *coYki -/-),* and ">" to indicate a promoter driving the expression of a gene (e.g., *EF1 >*
856 *coYki).*

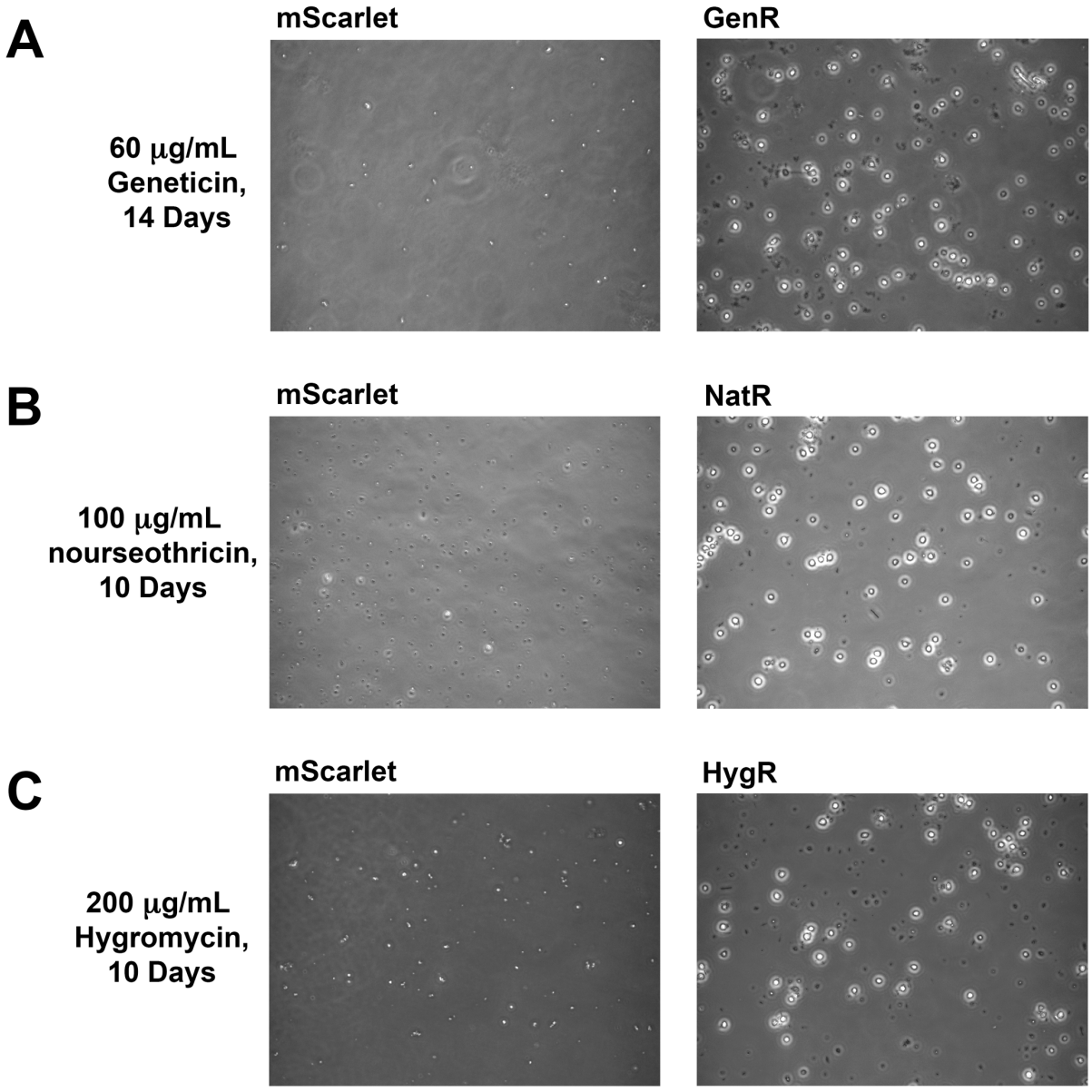

Fig. S1. Transfection of *Capsaspora* with genes encoding antibiotic resistance markers results in viable cell populations after drug treatment. Cells were transfected with plasmids encoding mScarlet with no antibiotic marker (pJP71), GenR (pJP72), NatR (pJP102), or HygR (pJP103) genes and were treated with the indicated antibiotics 2 days after transfection for the indicated time period. Representative images

of the population are shown. Round, phase-bright cells are visible in populations transfected with resistance markers but not cells transfected with mScarlet.

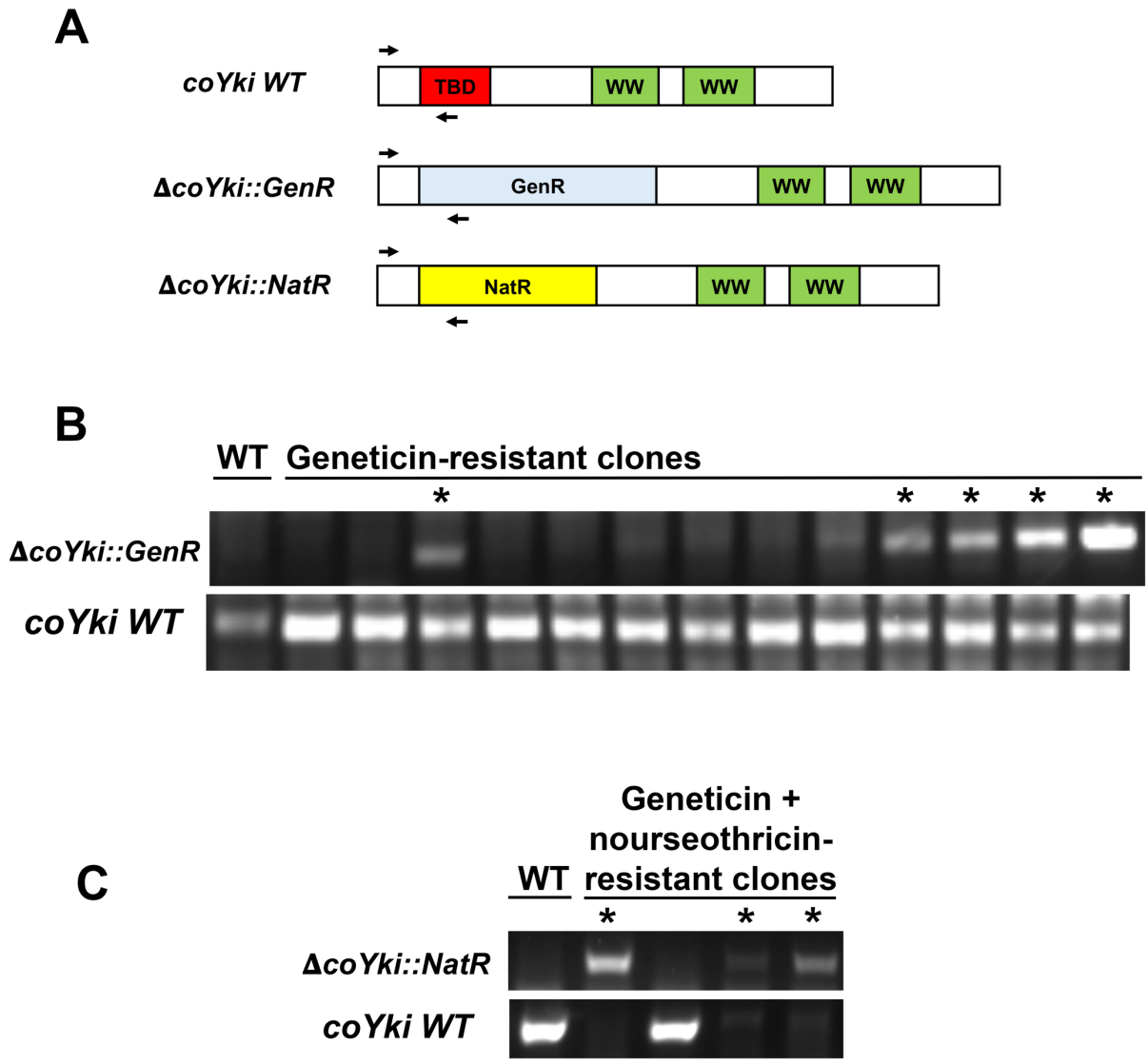

868

869

870 **Fig. S2. Diagnostic PCR of putative coYki deletion clonal cell lines. (A)** Diagram of
871 primer pairs used to evaluate the presence of the WT *coYki* allele (*coYki* WT), a deletion
872 of a region of *coYki* using the GenR marker (Δ*coYki::GenR*), or a deletion of a region of
873 coYki using the NatR marker (Δ*coYki::NatR*). TBD, Tead-binding domain; WW, WW
874 domain; GenR, Geneticin resistance; NatR, nourseothricin resistance. **(B)** WT cells were
875 transfected with a gene-targeting construct encoding GenR designed to delete the TBD

in the *coYki* gene by homologous recombination (see figure 1G in main text). Following transfection and drug selection, clonal populations of transfectants were generated and analyzed by diagnostic PCR using the indicated primer pairs. "*" indicates a clone showing a PCR product indicative of heterozygous coYki disruption. **(C)** A clonal cell line with a diagnostic PCR result indicating the disruption of a coYki allele with GenR was transfected with a gene-targeting construct encoding NatR designed to delete the TBD in the *coYki* gene. After selection with both Geneticin and nourseothricin, clonal populations of transfectants were generated and analyzed by diagnostic PCR using the indicated primer pairs. "*" indicates a clone showing a PCR product indicative of homozygous coYki disruption.

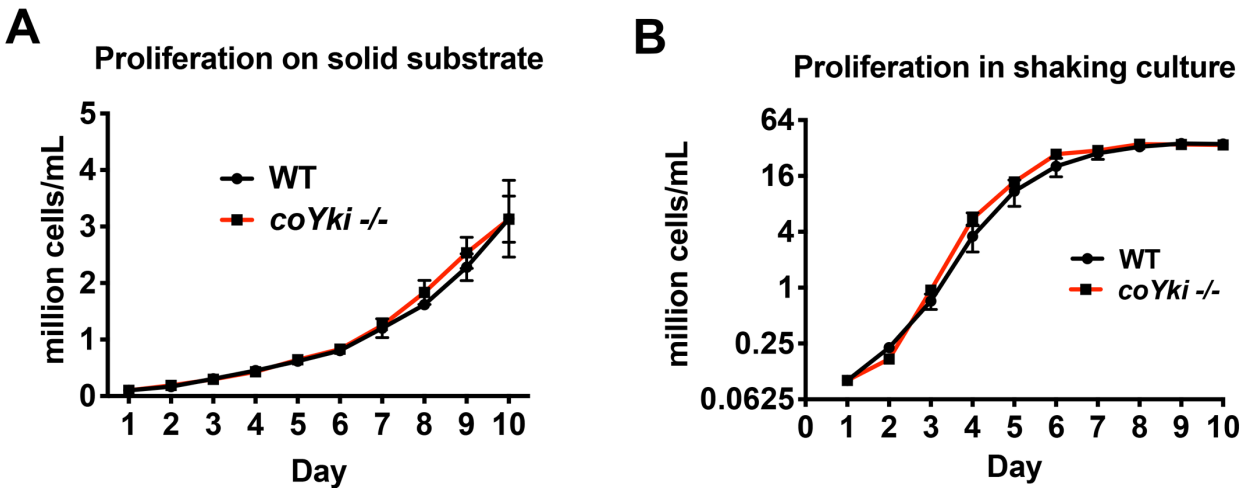

Fig. S3. WT and *coYki -/-* cells proliferate at a similar rate. (A) To examine proliferation on a solid substrate, cells were grown in wells in a 24-well plate, and each day cells within one well were resuspended and counted. **(B)** To examine proliferation in shaking culture, cells were grown in flasks on an orbital shaker, and an aliquot of cells was collected and counted daily. Values are mean ± SEM ($n \geq 3$). Absence of error bars indicates that error is smaller than the plot symbol.

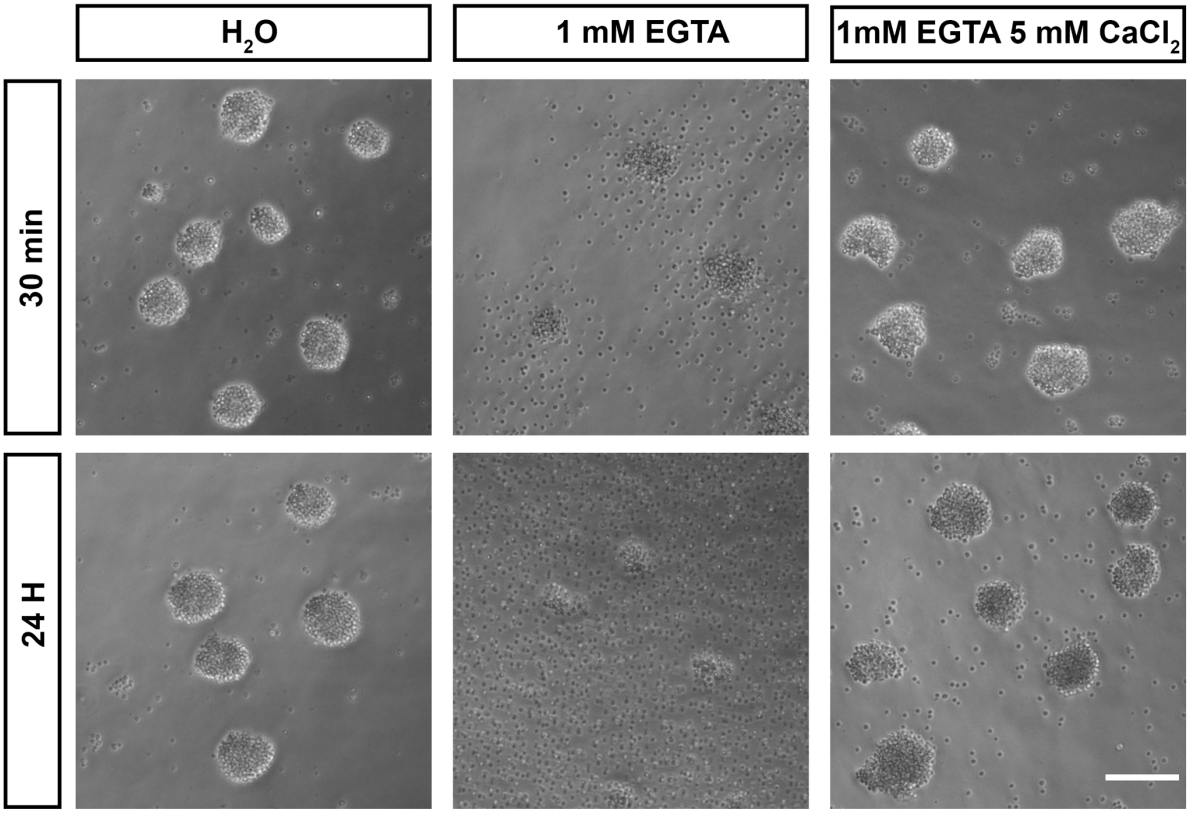

Fig. S4. Calcium is required for adhesion in *Capsapsora* cell aggregates. *Capsaspora* aggregates were treated with water (vehicle control), the calcium chelator EGTA, or EGTA with an excess of calcium. At 30 minutes aggregates treated with EGTA had begun to disassociate, with further disassociation evident at 24 hours. Simultaneous addition of an excess of calcium blocked this disassociation.

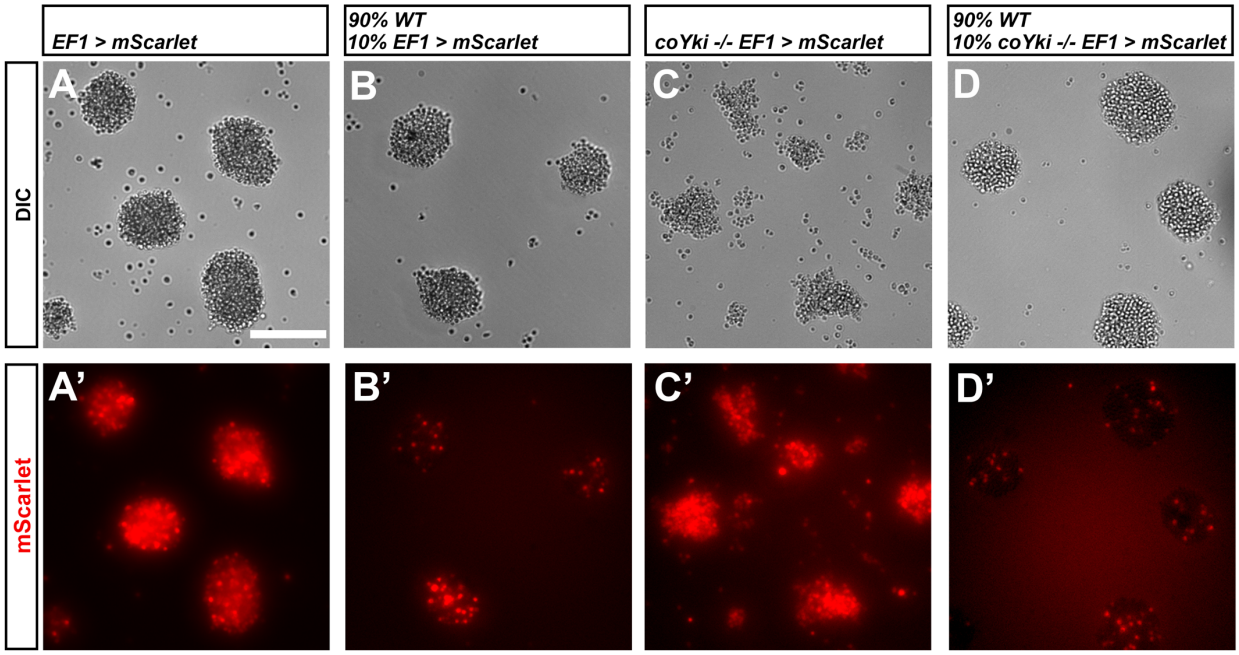

Fig. S5. *coYki -/-* cells adhere to and integrate within WT aggregates like WT cells. **(A-D)** Cells expressing mScarlet in the WT background **(A-B)** or in the *coYki -/-* mutant background **(C-D)** were allowed to aggregate as a homogeneous population **(A, C)** or were mixed with 90% WT cells and allowed to aggregate **(B, D)**. Individual mScarlet-labeled *coYki -/-* cells associate with WT cells within aggregates **(D')** in an organization like that of cells from the WT background labeled with mScarlet **(B')**. Scale bar is 75 microns.

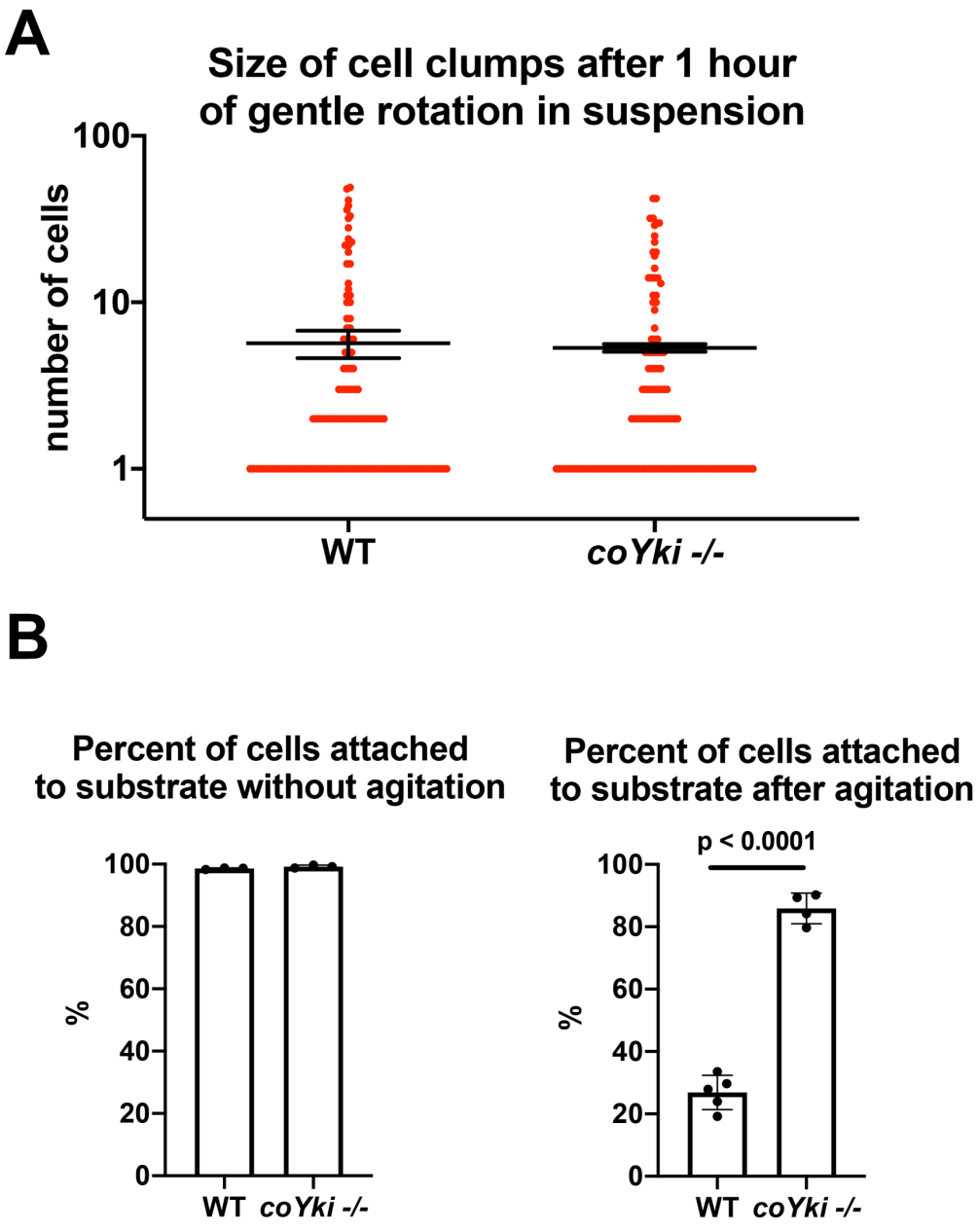

Fig. S6. coYki affects cell-substrate adhesion but shows no effect on cell-cell adhesion. (A) To examine cell-cell adhesion, cells in suspension were gently rotated for an hour to stimulate clump formation through cell-cell adhesion. Cultures were then examined by hemocytometer and the number of cells per clump was counted. Each red circle indicates the number of cells in a single clump, and error bars indicate the mean ± SEM of the average number of cells per clump from 3 independent experiments. Absence

of error bars indicates that error is smaller than the plot symbol. The difference in average number of cells per clump between WT and *coYki -/-* is not significant (t-test). **(B)** To examine cell-substrate adhesion, adherent cell cultures were either agitated on a rotary shaker for 10 minutes or left untreated, and then the number of adhered and unadhered cells in each culture was counted and the percent of cells adhered to the culture substrate was calculated. The difference between WT and *coYki -/-* is significant for the percent of cells attached to substrate after agitation ($p < 0.0001$, t-test).

Movie S1. Aggregation of WT or *coYki -/-* cells over 6 days on a low-adherence surface. Time units are given in days.

Movie S2. WT and *coYki -/-* cells on a glass surface.

Movie S3. *coYki -/-* cells expressing a *coYki* rescue transgene.

Movie S4. Basal region of *Capsaspora* cells expressing Lifeact-mScarlet.

Movie S5. Medial region of WT or *coYki -/-* cells expressing Lifeact-mScarlet.

Movie S6. Actin dynamics in a single *coYki -/-* cell expressing Lifeact-mScarlet.

Movie S7. WT or *coYki -/-* cells expressing Lifeact-mScarlet within an aggregate.

Movie S8. Treatment of *coYki -/-* cells expressing Lifeact-mScarlet with blebbistatin reduces blebbing.

951 **Data S1. Sequences of synthesized gene fragments used in this study**

952

953 **Data S2. Sequences of oligonucleotides used in this study**

954

955 **Data S3. Plasmids constructed for this study**